arXiv:hep-ph/9311263v3 29 Jan 1994

Preprint n.979
November 2, 1993
hep-ph/9311263
Revised version:
December 29, 1993

Dipartimento di Fisica
Università di Roma "La Sapienza"
I.N.F.N. - Sezione di Roma

Single Top Production at the Next Generation Linear e^+e^- Colliders

S. Ambrosanio[a,b,1] and B. Mele[b,a,2]

[a] *Dipartimento di Fisica, Università "La Sapienza", P.le Aldo Moro 2, I-00185 Rome, Italy*
[b] *I.N.F.N., Sezione di Roma, Italy*

Abstract

Present limits on the top mass from LEP1 and Tevatron point to a top quark that is considerably heavier than the W vector boson in the standard model. Hence, e^+e^- colliders with $\sqrt{s} \simeq 300$ GeV (the c.m. energy foreseen at the first phase of the Next Linear e^+e^- Collider) could be well below the energy threshold for real top-pair production. We argue that, if this is the case, single top production through the process $e^+e^- \to t\bar{b}W^-(\bar{t}bW^+)$, where $t\bar{b}(\bar{t}b)$ are produced mainly by means of a virtual W, becomes the dominant top production mechanism. Total cross sections and kinematical distributions are evaluated and numerical results are given in ranges of m_t and $\sqrt{s}$ where single top production can be of relevance. The relative importance of virtual-W and virtual-t contributions to the process is discussed.

[1] *e-mail address: AMBROSANIO@VAXROM.ROMA1.INFN.IT*

[2] *e-mail address: MELE@VAXROM.ROMA1.INFN.IT*

1. Introduction

The Next e^+e^- Linear Collider (NLC) will be an excellent place where to study precision top quark physics. The c.m. collision energy range at this machine is foreseen to be between 300 GeV (most probably in the first phase of operation) and 500 GeV, with a luminosity of the order of 10^{33} cm^{-2}s^{-1} [1, 2]. Top production at NLC will be very interesting both at the threshold region, where one expects some enhancement in the cross section due to the toponium resonance remnants, and in the continuum region [3]. At threshold, one can measure m_t with an accuracy better than 500 MeV. The shape of the excitation curve can be precisely predicted in perturbative QCD. Also, it will be quite sensitive to the perturbative strong coupling constant, the top width and Higgs boson mass and Yukawa coupling to the top quark. On the other hand, in the continuum top production well above the $\bar{t}t$ threshold, one will be able to test the $t \to bW^+$ coupling through the study of angular correlations in the $\bar{t}t$ decay products, as well as the existence of anomalies in the top couplings and possible non-standard top decay modes.

Although as yet unobserved, the existence of the top quark is strongly required by the theoretical consistency of the standard model. Direct search of top quark at Tevatron has yielded a lower limit $m_t > 113$ GeV at 95% C.L., for a top with standard-model decays [4]. The upgraded phase of the machine should either discover the top or exclude the mass range up to 160-180 GeV.

On the other hand, precision electroweak measurements from LEP1, M_W determination at hadron colliders and neutrino scattering constrain the top mass through radiative corrections in the range

$$m_t = \left(162^{+16+18}_{-17-21}\right)\ GeV \tag{1.1}$$

where the first error comes from experimental uncertainties and the second corresponds to varying the Higgs mass between 60 GeV and 1 TeV, with a central value of 300 GeV [5].

According to present limits on m_t, the top mass could well be in the range (150-200) GeV. If this were the case, in the first phase of NLC corresponding to a c.m. energy of about 300 GeV, the collision energy could be not sufficient for top-pair production. In this situation, since the top is considerably heavier than the W vector boson, top quarks are mainly produced in association with a W and a b quark through

$\mathbf{m_t}$ (GeV)	**120**	**130**	**140**	**150**	**160**	**170**	**180**	**190**	**200**
$\sqrt{\mathbf{s}} = \mathbf{300\ GeV}$	1.37	1.16	0.85	–	––	––	––	––	––
320	1.31	1.17	0.99	0.72	–	––	––	––	––
340	1.23	1.13	1.01	0.85	0.62	–	––	––	––
360	1.14	1.07	0.98	0.88	0.74	0.54	–	––	––
380	1.05	1.00	0.94	0.86	0.77	0.64	0.47	–	––
400	0.97	0.93	0.89	0.83	0.76	0.68	0.57	0.41	–
450	0.80	0.78	0.75	0.72	0.69	0.65	0.60	0.54	0.47
500	0.66	0.65	0.64	0.62	0.60	0.58	0.55	0.52	0.49

Table 1: Total cross section (in pb) for the process $e^+e^- \to \bar{t}t$ at the Born level.

the processes

$$\begin{aligned} e^+e^- &\to t\bar{b}W^- \\ e^+e^- &\to \bar{t}bW^+. \end{aligned} \tag{1.2}$$

In fig.1, we show the Feynman diagrams corresponding to $e^+e^- \to t\bar{b}W^-$ (charge conjugated graphs correspond to the reaction $e^+e^- \to \bar{t}bW^+$). Aside the tt^* channel that is responsible for top pair production above threshold, in single top production also bb^* and WW^* channels, where a virtual b quark and W respectively are exchanged, contribute to the cross section. In particular, the WW^* turns out to be the dominant contribution in almost the whole interesting $\sqrt{s}$ range, that is $m_t + M_W + m_b \leq \sqrt{s} \leq 2m_t$. Of course, cross sections are $\mathcal{O}(\alpha_W^3)$ and therefore quite smaller than those relative to top pair production (reported in Table 1) which are of the order of 1 pb at NLC (cf. ref.[6]).

In the present work we make a detailed study of single top production in e^+e^- collisions below the $\bar{t}t$ threshold, namely when $\sqrt{s} < 2m_t$. We mainly refer to the practical case of NLC with $\sqrt{s} \simeq 300$ GeV and an integrated luminosity of 10 fb^{-1}, but also other possibilities for the e^+e^- collision energy are considered. As far as the top mass is concerned, we focus on the range $150 \lesssim m_t \lesssim 200$ GeV, with $m_t > \sqrt{s}/2$.

We will neglect throughout our study toponium resonance effects near the $\bar{t}t$ threshold.

As anticipated, cross sections are found to be rather moderate (of the order of a few fb's) and marginal for the study of top properties at the foreseen NLC luminosity. Nevertheless, single top production could be a relevant background for rare processes and possible new physics signal at future e^+e^- colliders. In fact, as a result of the fast top decay, one observes a $W^+W^-\bar{b}b$ final state, that is a possible background for any process involving multi-vector boson production. For instance, standard-model processes like $e^+e^- \to WWZ$ [7] and $e^+e^- \to WWH$ [8] involve the same final state. Also, analogous signals could correspond to new physics effects, e.g. chargino production in supersymmetric models [9].

Single top production in e^+e^- collisions through the process $e^+e^- \to t\bar{b}e^-\bar{\nu}_e$ was considered in ref.[10] for $m_t =$ (30-60) GeV at PETRA and TRISTAN energies. With this kinematical configuration, a real W in the final state (as in $e^+e^- \to t\bar{b}W^-$) is not allowed and single top production occurs mainly through the higher-order reaction $\gamma e^+ \to t\bar{b}\bar{\nu}_e$, where an almost-real photon is radiated by the initial e^- beam. Therefore, the corresponding production rates are quite small (and undetectable). For instance, at $\sqrt{s} = 50$ and 65 GeV total cross sections of 1.1×10^{-5} fb and 2.9×10^{-3} fb, respectively, are found for $m_t = 40$ GeV.

After completion of our work, we learnt of two recent studies concerning single top production at LEP200 [11, 12]. In ref.[11], analytical expressions for cross sections of the reaction $e^+e^- \to t\bar{b}e^-\bar{\nu}_e$ are given for the photon initiated process, as well as for the WW^* and tt^* contributions (where $W \to e\nu$). Unfortunately, below the $\bar{t}t$ threshold, event rates are found to be too small for m_t larger than the present Tevatron limit, even for c.m. energies of 220-250 GeV (that are, however, well above the foreseen $\sqrt{s}$ at LEP200). In this work, as in ref.[10], the authors concentrate on $e\nu$ final states, that replace the real W in the reaction $e^+e^- \to t\bar{b}W^-$. This is because with the LEP200 c.m. energy, for most of the interesting m_t range, one can not afford to produce a top quark plus a *real* W. Hence, the higher-order $\gamma e^+ \to t\bar{b}\bar{\nu}_e$ process becomes the dominant channel. Instead, in the case of $e^+e^- \to t\bar{b}W^-$ at higher c.m. energies, that we consider here, the final $e\nu$ state can be replaced by other leptonic and hadronic decays of the W, that are equally interesting and increase the production rate. As far as tt^* and WW^* channels are concerned, we compared the output of our programs with the results of ref.[11] and found complete agreement at LEP200 energies.

In ref.[12], a similar study for single top production at LEP200 has been carried

out with drastically different results with respect to ref.[11]. We think that such disagreement is due to a mis-treatment of the photon collinear singularity in the process $e^+e^- \to t\bar{b}e^-\bar{\nu}_e$ that largely overestimates the contribution from diagrams with a photon exchange in the t-channel.

We stress that the NLC regime, that we are considering here, will provide for the first time the environment to study single top production *at the leading order* and with observable rates. Furthermore, contrary to the previous studies, we include the bb^* contribution and study in detail kinematical distributions.

After a short description of our computation method, in section 2, we will discuss the behaviour of total cross sections for the reaction $e^+e^- \to t\bar{b}W^-(\bar{t}bW^+)$ versus $\sqrt{s}$ and m_t, stressing the relative importance of various contributions to the matrix element squared. In section 3, we will study the distribution in the Wb invariant mass and the angular distribution of the top with respect to the beam. Once more, contributions from different diagrams will be emphasized. In section 4, we will give our conclusions.

2. Total cross sections

In fig.1, the seven Feynman diagrams contributing to the process $e^+e^- \to t\bar{b}W^-$ at tree level are shown. As a result, one has 28 terms, including interferences, in the expression for the matrix element squared.

Aside the graphs $\mathbf{a}_{1,2}$, that correspond to the relevant diagrams for production of a pair of real top quarks, here we have b- and W-exchange diagrams, where the top quark comes from the decay of a virtual b quark and W vector boson respectively. In the latter case, aside the γ and Z contributions, we have a further graph coming from W-pair production through neutrino exchange in the t-channel. Note that the virtual W and, to a greater extent, b momenta in $\mathbf{b}_i$- and $\mathbf{c}_i$-type diagrams are always far from their mass shell, since an heavy top has to be produced. As for the $\mathbf{a}_i$-type graphs, if the c.m. energy is above the $\bar{t}t$ threshold, they reproduce real $\bar{t}t$ production with subsequent $\bar{t} \to \bar{b}W^-$ decay on the $\bar{t}$ mass shell. Hence, the corresponding contribution turns out to be quite enhanced. On the other hand, when $\sqrt{s}$ is well below the $\bar{t}t$ threshold, the contributions from virtual-W (and -b) exchange could be, in a first qualitative approach, not negligible with respect to the t exchange. Indeed, we will show that W exchange is dominant for most of the $\sqrt{s}$ range of interest for

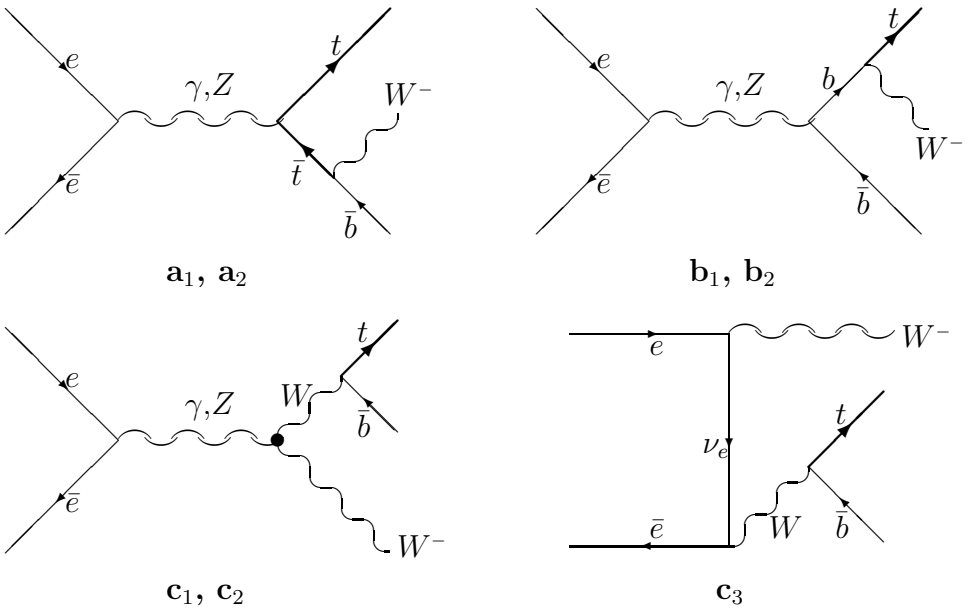

Fig. 1: Feynman diagrams for the process $e^+e^- \to t\bar{b}W^-$. a_i: diagrams with top exchange, b_i: diagrams with b-quark exchange, c_i: diagrams with W exchange. $i = 1$: γ exchange in the s-channel, $i = 2$: Z^0 exchange in the s-channel, $i = 3$: ν_e exchange in the t-channel.

single top production.

Numerical results for total cross sections and distributions for the process $e^+e^- \to t\bar{b}W^-$ have been obtained in the following way. We used the program CompHEP 2.3-5 [13] in order to get the matrix element squared for $e^+e^- \to t\bar{b}W^-$ at the Born level, in a symbolic form and in a FORTRAN compatible form as well. Then we developed some software (based on VEGAS [14]), performing a numerical Monte Carlo phase space (p.s.) integration over the three-massive-particle final state with three different masses. We chose the VEGAS input parameters in such a way as to obtain a three-digit accuracy on the p.s. integration, that is 3-dimensional for distributions and 4-dimensional for total cross sections. Firstly, we performed the p.s. integration on the solid angles of the Wb system in its c.m. frame. The relevant formula for the invariant distributions for top variables is then

$$D_{top} = E_t \frac{d^3\sigma}{d\mathbf{p}_t} = \frac{\beta_W}{(4\pi)^5 s} \left(1 + \frac{M_W^2 - m_b^2}{M_{Wb}^2}\right) \int \overline{|\mathcal{M}|^2}\, d\cos\theta_W\, d\phi_W \qquad (2.1)$$

where

$$\beta_W = \sqrt{1 - 4\frac{M_{Wb}^2 M_W^2}{(M_{Wb}^2 + M_W^2 - m_b^2)^2}}. \tag{2.2}$$

M_{Wb} is the invariant mass of the Wb system, which is linked to the top energy, E_t, in the e^+e^- c.m. system by

$$M_{Wb} = \sqrt{s + m_t^2 - 2\sqrt{s}E_t}, \tag{2.3}$$

and θ_W, ϕ_W are the polar and azimuthal angle of the W with respect to the e^- beam direction in the Wb rest frame. In eq.(2.1), the squared matrix element $\overline{|\mathcal{M}|^2}$ (averaged over initial and final particle polarizations) for the process $e^+e^- \to t\bar{b}W^-$ has been expressed in terms of θ_W, ϕ_W, M_{Wb} and $\cos\theta_t$, where θ_t is the angle between the top 3-momentum and the e^- one, in the e^+e^- c.m. frame. Then, one has

$$\frac{d^2\sigma}{dM_{Wb}\, d\cos\theta_t} = 2\pi|\mathbf{p}_t|\frac{M_{Wb}}{\sqrt{s}}D_{top} \tag{2.4}$$

At this point, total cross sections are obtained by performing the remaining two integrations over M_{Wb} and $\cos\theta_t$. We checked the stability of the numerical integration by choosing different sets of independent kinematical variables. We found that the above choice is a very good one in order to optimize the estimated relative error on total cross section. Furthermore, we found that the choice of the integration variable M_{Wb} has a crucial role in reproducing cross sections above the $\bar{t}t$ pair threshold, starting from single top production formulae. Indeed, above the $\bar{t}t$ threshold the bulk of the cross section comes from the pole corresponding to $M_{Wb} \simeq m_t$ in the t propagator in diagrams $\mathbf{a}_{1,2}$.

In our computation, we used the following set of parameter values

$$\begin{aligned}
M_Z &= 91.18\ GeV, & M_W &= 80.1\ GeV, \\
\Gamma_Z &= 2.49\ GeV, & \Gamma_W &= 2.12\ GeV, \\
m_b &= 5.00\ GeV, & \alpha_{EM} &= 1/128\ , \\
\sin^2\theta_W &= 0.232\ , & V_{tb} &= 0.999\ .
\end{aligned}$$

The precise value of the top width Γ_t, which enters the amplitudes relative to the graphs $\mathbf{a}_{1,2}$ through the top propagator $1/(p^2 - m_t^2 + im_t\Gamma_t)$, is not important when one considers $e^+e^- \to t\bar{b}W^-$ well below the $\bar{t}t$ threshold. On the contrary, if one extends the $e^+e^- \to t\bar{b}W^-$ formulae to values of $\sqrt{s}$ around and above the $\bar{t}t$ threshold, (i.e. integrates over the pole in the top propagator), the results for cross section are

$\mathbf{m_t}$ **(GeV)**	**120**	**130**	**140**	**150**	**160**	**170**	**180**	**190**	**200**
$\Gamma(t \to bW)\ (GeV)$	0.327	0.485	0.671	0.885	1.13	1.41	1.71	2.06	2.44

Table 2: Top quark width in the Born approximation for several values of m_t.

rather sensitive to the value of Γ_t. In order to recover through our computation also the Born cross sections for real $\bar{t}t$ production at $\sqrt{s} \gtrsim 2m_t$, we have approximated the top total width with the tree level width for $t \to Wb$ [1] [16]:

$$\Gamma_t \simeq \Gamma(t \to bW) \simeq \frac{G_F m_t^3}{8\pi\sqrt{2}} \left(1 - \frac{M_W^2}{m_t^2}\right)^2 \left(1 + 2\frac{M_W^2}{m_t^2}\right). \tag{2.5}$$

In this way, starting from our formulae for $e^+e^- \to t\bar{b}W^-$, to a very good approximation, we obtain for $\sqrt{s} \geq 2m_t$

$$\sigma(Wtb) = \sigma(\bar{t}t) \cdot BR(t \to Wb) \simeq \sigma(\bar{t}t), \tag{2.6}$$

where $\sigma(\bar{t}t)$ is the tree level cross section for $e^+e^- \to \bar{t}t$ reported in Table 1.

Values of Γ_t obtained through eq.(2.5) are shown versus m_t in Table 2.

In our computation, we will not take into account resonance effects near $\bar{t}t$ threshold and, as a consequence, our results can be trusted only when $2m_t - \sqrt{s} \gg \Gamma_t$ below threshold. In practice, our results should be rather accurate at tree level in the region $\sqrt{s} \lesssim 2m_t - 3\Gamma_t$ and $\sqrt{s} \gtrsim 2m_t$.

Total cross sections for $e^+e^- \to t\bar{b}W^-$ are presented in Table 3 and in figs.2-4. In Table 3 we report the numerical results of our programs (in fb), summing up over both $e^+e^- \to t\bar{b}W^-$ and $\bar{t}bW^+$ contributions. We restrict ourselves to the range $150 \leq m_t \leq 200$ GeV and $240 \leq \sqrt{s} \leq 400$ GeV, thus including in our study the possibility of intermediate e^+e^- collision energies between LEP200 and NLC at $\sqrt{s} = 300$ GeV.

In Table 3, results are shown only for $m_t + M_W + m_b < \sqrt{s} < 2m_t$, that is where single top production is the dominant top production mechanism. Here, cross

[1] Note that $\Gamma(t \to bW) \simeq 0.998\Gamma_t^{TOT}$ irrespective of m_t (for $m_t \gtrsim 120$ GeV) and that the inclusion of QCD, electroweak radiative corrections and finite W-width effects decreases Γ_t by about 8-9% [15].

$\mathbf{m_t}$ **(GeV)**	**150**	**160**	**170**	**180**	**190**	**200**
$\sqrt{\mathbf{s}} = \mathbf{240\ GeV}$	0.018	$--$	$--$	$--$	$--$	$--$
260	0.89	0.19	0.010	$--$	$--$	$--$
280	4.2	1.5	0.50	0.11	0.006	$--$
300	$\bar{t}t$	5.2	2.2	0.90	0.31	0.070
320	$\bar{t}t$	$\bar{t}t$	6.3	2.8	1.3	0.59
340	$\bar{t}t$	$\bar{t}t$	$\bar{t}t$	7.2	3.4	1.8
360	$\bar{t}t$	$\bar{t}t$	$\bar{t}t$	$\bar{t}t$	8.1	4.0
380	$\bar{t}t$	$\bar{t}t$	$\bar{t}t$	$\bar{t}t$	$\bar{t}t$	9.0
400	$\bar{t}t$	$\bar{t}t$	$\bar{t}t$	$\bar{t}t$	$\bar{t}t$	$\bar{t}t$

Table 3: Total cross section (in fb) for single top production. Contributions from both $e^+e^- \to t\bar{b}W^-$ and $\bar{t}bW^+$ processes are considered. Entries in the range $\sqrt{s} \geq 2m_t$, where top-pair production is dominant, are marked by "$\bar{t}t$".

sections turn out to be about two orders of magnitude smaller than those for top-pair production above threshold (cf. Table 1). In particular, by varying m_t from 150 GeV up to 200 GeV, one gets cross sections from 4 to 9 fb for $\sqrt{s} = 2m_t - 20$ GeV and from 0.9 to 4 fb for $\sqrt{s} = 2m_t - 40$ GeV. For 180 GeV $< m_t <$ 200 GeV, we still have cross sections of the order of 1 fb or more for $\sqrt{s} = 2m_t - 60$ GeV. Assuming an integrated luminosity of 10 fb^{-1}, this corresponds to the production of 10-100 single top events. Hence, even after inclusion of experimental cuts and efficiencies, one should get observable single top event rates.

In fig.2, the behaviour of various contributions to the cross section versus $\sqrt{s}$, in the region below the $\bar{t}t$ threshold, is shown for $m_t = 160$ GeV (fig.2a) and $m_t = 200$ GeV (fig.2b). Squares represent the contribution to the total cross section coming from diagrams $\mathbf{a}_{1,2}$ in fig.1, in which a virtual top is exchanged, while the circles stand for the virtual-W contribution, namely the one coming from diagrams $\mathbf{c}_{1,2,3}$. Thunders account for virtual-top and virtual-W diagrams (including interferences between the two). Finally, the solid line refers to the complete computation that takes into account all diagrams in fig.1.

Fig.2 shows very clearly that the contribution of virtual-W diagrams is very important. Indeed, it is larger than the one from virtual-top diagrams for $\sqrt{s} \lesssim 2m_t -$

Fig. 2: Various contributions to the total cross section of for $e^+e^- \to t\bar{b}W^-$ when $m_t + M_W + m_b \leq \sqrt{s} \leq 2m_t$. a) $m_t = 160$ GeV; b) $m_t = 200$ GeV.
Squares and circles represent respectively contributions from diagrams with virtual-top and virtual W-exchange. Thunders account for both the previous two (plus interferences). The solid line shows total cross section including all contributions in fig.1.

Fig. 3: Various contributions to the total cross section of the process $e^+e^- \to t\bar{b}W^-$ for $\sqrt{s} = 300$ GeV. Notations are the same as in fig.2.

$(7 \div 10)\Gamma_t$. The latter can be even neglected for still lower $\sqrt{s}$, where it is about an order of magnitude lower than the virtual-W contribution. On the other hand, the contribution coming from diagrams $\mathbf{b}_{1,2}$ with virtual-b exchange is very small everywhere. For this reason, in our plots the thunders are well superimposed to the solid line. This is due to the b-quark propagator suppression of the amplitudes relative to diagrams $\mathbf{b}_{1,2}$, since the b^* has to decay in a heavy tW final state. Concerning interferences between virtual-top and virtual-W diagrams, they are destructive and in general small. This is no more true in the $\sqrt{s}$ region below the $\bar{t}t$ threshold by few Γ_t's, where virtual-top and virtual-W contributions becomes both sizable and comparable.

In fig.3, the various contributions to total cross section are analyzed as functions of m_t, for fixed $\sqrt{s} = 300$ GeV, that could be of interest for the first phase of NLC operation. One can see that, when $m_t \gtrsim 165$ GeV, considering only the virtual-W contribution is a very good approximation for the total cross section. In particular, for $165 \lesssim m_t \lesssim 190$ GeV the usual tt^* contribution would underestimate the production rates by a factor from 3 to 10. After the $\bar{t}t$ threshold region, where the virtual-top

Fig. 4: Various contributions to the total cross section of the process $e^+e^- \to t\bar{b}W^-$ for $m_t = 180$ GeV and $\sqrt{s} \geq 2m_t$. Notations are as in fig.2.

contribution dominates, we have an intermediate m_t range, $155 \lesssim m_t \lesssim 160$ GeV, where the virtual-top and virtual-W contributions are separately comparable and have destructive interference in the total.

Of course, event rates decrease when m_t grows. At $\sqrt{s} = 300$ GeV, with an integrated luminosity of 10 fb^{-1} and summing over t and $\bar{t}$ events, one can hope to detect through single top production a top quark with m_t up to about 185 GeV.

In fig.4, we plot the $e^+e^- \to t\bar{b}W^-$ cross section versus $\sqrt{s}$ above the $\bar{t}t$ threshold and up to $\sqrt{s} = 2$ TeV, for $m_t = 180$ GeV. Of course, $\sigma(\bar{t}t)$ is recovered in this case, since we assumed BR$(t \to Wb) \simeq 1$. Note that, although in general negligible in this case, the relative importance of single top production through virtual-W increases at high energies. Indeed, as the contribution of $\mathbf{a}_{1,2}$ diagrams in fig.1 quickly decreases after crossing the $\bar{t}t$ threshold peak, the contribution of $\mathbf{c}_{1,2,3}$ diagrams keeps growing up to $\sqrt{s} \simeq 1$ TeV and then starts to decrease rather slowly. This is due mainly to the presence of trilinear boson vertex in the diagram $\mathbf{c}_3$. As a result, e.g. we have that at $\sqrt{s} = 2$ TeV the cross section for single top production through a virtual W only would be about one third of the continuum $\bar{t}t$ cross section. In reality, in this

Fig. 5: Distribution in the invariant mass of the Wb system M_{Wb} for $e^+e^- \to t\bar{b}W^-$ when $m_t = 180$ GeV and: a) $\sqrt{s} = 280$ GeV; b) $\sqrt{s} = 310$ GeV; c) $\sqrt{s} = 350$ GeV; d) $\sqrt{s} = 370$ GeV.

energy region there is a large interference effect between WW^* and tt^* diagrams that restores almost completely the usual $\bar{t}t$ cross section coming from the production of two real top quarks (cf. fig.4).

3. Kinematical distributions

In this section, we study kinematical distributions that characterize the final state in single top production. Particular emphasis is given to the comparison with analogous distributions above the $\bar{t}t$ threshold. In fig.5, distributions in the Wb invariant

mass M_{Wb} for the process $e^+e^- \to t\bar{b}W^-$ are shown for $m_t = 180$ GeV and different values of $\sqrt{s}$, below or just above the $\bar{t}t$ threshold ($\sqrt{s} = 280,\ 310,\ 350,\ 370$ GeV in figs.5a,b,c,d respectively). The curves are normalized in such a way as to be adimensional and to have an integral equal to 1 when integrated over the whole M_{Wb}/m_t range, that is

$$\frac{M_W + m_b}{m_t} \leq \frac{M_{Wb}}{m_t} \leq \frac{\sqrt{s}}{m_t} - 1. \tag{3.1}$$

Well under the $\bar{t}t$ threshold, the M_{Wb} distribution is rather broad and has a maximum at values much lower than m_t. This is due to the dominance in this region of virtual-W contributions, for which the invariant mass of the Wb pair is not correlated to m_t or to any other resonance. Then, as the c.m. energy approaches the $\bar{t}t$ threshold, one has the progressive appearance of the $\bar{t}$-resonance peak at $M_{Wb} \simeq m_t$, with increasingly small tails at lower M_{Wb}. This, of course, is due to the t^* propagator in the virtual-top diagrams, that dominate onto other contributions near and above the $\bar{t}t$ threshold, where most of the cross section comes from the production of a real top and consequent decay in Wb.

The comparison of different contributions to the M_{Wb} distribution is more clearly shown in fig.6, for $m_t = 150$ GeV. In fig.6a, one can see that below the $\bar{t}t$ threshold the M_{Wb} distribution is dominated by the flatter virtual-W contribution. Note that even above the $\bar{t}t$ threshold (cf. fig.6b, where $\sqrt{s} = 500$ GeV), when the bulk of cross section is concentrated at $M_{Wb} \simeq m_t$, single top production through the virtual-W contribution gives a predominant contribution to the $e^+e^- \to t\bar{b}W^-$cross section in the large Wb invariant mass region. Indeed, the virtual-W tail gets about an order of magnitude larger than the tt^* one for $M_{Wb} \simeq 2m_t$ in fig.6b. Anyway, the corresponding rates will be hardly observable with the foreseen NLC luminosity.

An analogous transition from the "WW^* dominance" to the "tt^* dominance" can be observed in the angular distribution for the top quark in $e^+e^- \to t\bar{b}W^-$ with respect to the e^- beam direction. In fig.7, we set $m_t = 180$ GeV and $\sqrt{s} = 280,\ 310,\ 350,\ 370$ GeV (figs.7a,b,c,d respectively). By varying $\sqrt{s}$, one can see that two different behaviours compete. At low $\sqrt{s}$, a collinear t to the e^+ beam is favoured and prevails in the region well below the $\bar{t}t$ threshold (fig.7a,b). On the other hand, as $\sqrt{s}$ approaches $2m_t$, $d\sigma/d\cos\theta_t$ is enhanced in the positive $\cos\theta_t$ region, and top quarks that are collinear to the e^- are dominant.

Fig.8 shows that the virtual-W contribution is responsible for the first effect while virtual-t diagrams produce rather forward-peaked top quarks along the e^- beam. In

Fig. 6: Various contributions to the distribution for the invariant mass M_{Wb} in the case $m_t = 150$ GeV. a) $\sqrt{s} = 270$ GeV, b) $\sqrt{s} = 500$ GeV. Notations are as in fig.2.

Fig. 7: Angular distribution for the top quark in $e^+e^- \to t\bar{b}W^-$ with respect to the e^- beam direction, in the case $m_t = 180$ GeV and:
a) $\sqrt{s} = 280$ GeV; b) $\sqrt{s} = 310$ GeV; c) $\sqrt{s} = 350$ GeV; d) $\sqrt{s} = 370$ GeV.

Fig. 8: Various contributions to $\cos\theta_t$ distribution in the case $m_t = 150$ GeV.
a) $\sqrt{s} = 290$ GeV, b) $\sqrt{s} = 1$ TeV. Notations are as in fig.6.

fact, what one observes in $d\sigma/d\cos\theta_t$ reflects the differences in the angular distributions for the "parent" processes $e^+e^- \to W^+W^-$ and $e^+e^- \to \bar{t}t$. In $e^+e^- \to W^+W^-$, the W^+ is produced preferentially along the e^+ direction (see, e.g., ref.[17]). The top quark produced through the virtual-W diagrams in $e^+e^- \to t\bar{b}W^-$ and coming from the W^* decay, due to its heaviness, well reflects the would-be final W^+ direction in $e^+e^- \to W^+W^-$. Hence, the top from WW^* will be preferentially along the e^+ direction too. On the contrary, the t quark produced in the tt^* channel reflects the t angular distribution in $e^+e^- \to \bar{t}t$, that is always peaked toward the e^- direction [6].

In fig.8, the case $m_t = 150$ GeV is considered in the region just below the threshold ($\sqrt{s} = 290$ GeV, fig.8a), where the WW^* and tt^* contributions are comparable, and at very high c.m. energy ($\sqrt{s} = 1$ TeV, fig.8b). In the latter case, it is possible to distinguish a small peak at $\cos\theta_t = -1$ due to the relative enhancement at high $\sqrt{s}$ of the virtual-W contribution (cf. fig.4).

4. Summary and conclusions

In this paper, we have studied single top production in e^+e^- collisions through the processes $e^+e^- \to t\bar{b}W^-$, $\bar{t}bW^+$, considering aside the tt^* channel, that is relevant for top pair production, WW^* and bb^* channels, with $W^* \to tb$ and $b^* \to tW$ respectively. Since present limits on m_t imply that the top is considerably heavier than the W vector boson, this process will be of relevance for top production at Next Linear e^+e^- Colliders operating at a c.m. energy below the $e^+e^- \to \bar{t}t$ threshold. This, for instance, will be the case if the top is heavier than 150 GeV for a NLC with $\sqrt{s} \simeq 300$ GeV or less. We found that, assuming an integrated luminosity of about 10 fb^{-1}, production rates are sufficient to detect a top signal below the $\bar{t}t$ threshold for a large fraction of the kinematically allowed energy window $m_t + M_W + m_b < \sqrt{s} < 2m_t$. In particular, considering e^+e^- collisions at $240 \lesssim \sqrt{s} \lesssim 400$ GeV, by varying m_t from 150 GeV up to 200 GeV, we get cross sections from 4 to 9 fb for $\sqrt{s} = 2m_t - 20$ GeV and from 0.9 to 4 fb for $\sqrt{s} = 2m_t - 40$ GeV. For $180 < m_t < 200$ GeV, one still obtains cross sections of the order of 1 fb or more for $\sqrt{s} = 2m_t - 60$ GeV. The above rates include both the single t and $\bar{t}$ production.

Invariant Wb mass distributions and top angular distributions have been studied and kinematical differences with respect to the $\bar{t}t$ pair production above threshold have been stressed.

The relative importance of the tt^*, WW^* and bb^* contributions has been extensively studied both for cross sections and kinematical distributions . We found that the virtual-W exchange is predominant in the total cross section for $\sqrt{s} \lesssim 2m_t - 20$ GeV. For instance, if $m_t = 200$ GeV, WW^* contribution is more than one order of magnitude larger than the tt^* one for $\sqrt{s} \lesssim 320$ GeV. Consequently, also the kinematical features of the final states are governed by the WW^* channel well below the $\bar{t}t$ threshold. We have a rather broad M_{Wb} distribution that reflects the non-resonant structure of the Wb final state, as opposed to the tt^* case. Furthermore, the top angular distribution recalls the W^+ one in the process $e^+e^- \to W^+W^-$ that is quite opposite to the t distribution coming from the tt^* contribution.

We also found that, due basically to the different behaviour of the $e^+e^- \to \bar{t}t$ and $e^+e^- \to W^+W^-$ cross sections versus $\sqrt{s}$, single top production mediated by a virtual W can be non-negligible far above the $\bar{t}t$ threshold (cf. fig.4), although tt^* and WW^* interference effects tend to cancel the eventual increase in the total top production rate. However, for $\sqrt{s} \simeq$ 1-2 TeV and sufficiently large luminosity, some WW^* effect could be detectable by studying distributions in particular ranges of kinematical variables (cf. fig.8b).

Regarding the bb^* contribution to the $e^+e^- \to t\bar{b}W^-$ cross section, this is found to be always negligible.

As far as detection of a $e^+e^- \to t\bar{b}W^-$ signal is concerned, as a result of the fast top decay, one observes a $W^+W^-\bar{b}b$ final state. Hence, the study of single top production rates below the $\bar{t}t$ threshold are interesting not only by itself. A detailed knowledge of this process also leads to a better determination of the possible background for any process of moderate cross section involving multi-vector boson final states.

Acknowledgements

We are indebted to S. Ilyin and A. Pukhov for useful discussions on the CompHEP software.

References

[1] Proc. of the 2^{nd} International Workshop on "Physics and Experiments with Linear e^+e^- Colliders", Waikoloa, Hawaii, April 26-30, 1993 (in preparation).

[2] Proc. of the 2^{nd} Workshop "e^+e^- Collisions at 500 GeV: The Physics Potential", Munich, Annecy, Hamburg, Nov 20, 1992 - Apr 3, 1993, ed. P.M. Zerwas, DESY 92-123C (1994) (in preparation).

[3] P.M. Zerwas, in the Proc. of the 1^{st} International Workshop on "Physics and Experiments with Linear e^+e^- Colliders", Saariselkä, Finland, 9-14 Sep 1991, eds. R. Orava, P. Eerola, M. Nordberg, p.165 and references therein.

[4] talks by P. Tipton (CDF collaboration) and N. Hadley (D0 collaboration) at the XVI Int. Symp. on Lepton-Photon Interactions, Cornell University, Ithaca, N.Y., U.S.A., August 10-15, 1993.

[5] plenary talk by J. Lefrançois at the Int. Europhysics Conf. on High Energy Physics, Marseille, July 22-28, 1993.

[6] W. Bernreuther et al., in the Proc. of the 1^{st} Workshop "e^+e^- Collisions at 500 GeV: The Physics Potential", Munich, Annecy, Hamburg, Feb 4-Sep 3, 1991, ed. P.M. Zerwas, DESY 92-123A (1992), p.255.

[7] V. Barger, T. Han and R.J.N. Phillips, Phys. Rev. **D39** (1989) 146.

[8] M. Baillargeon, F. Boudjema, F. Cuypers, E. Gabrielli and B. Mele, preprint CERN-TH-6932-93, ENSLAPP-A-425-93, LMU-10-93, June 1993.

[9] A. Bartl and W. Majerotto, in the Proc. of the 2^{nd} Workshop "e^+e^- Collisions at 500 GeV: The Physics Potential", Munich, Annecy, Hamburg, Nov 20, 1992 - Apr 3, 1993, ed. P.M. Zerwas, DESY 92-123C (1994) (in preparation).

[10] M. Katuya, J. Morishita, T. Munehisa and Y. Shimizu, Prog. Theor. Phys. **75** (1986) 92.

[11] O. Panella, G. Pancheri and Y.N. Srivastava, Phys. Lett. **B318** (1993) 241.

[12] M. Raidal and R. Vuopionperä, Phys. Lett. **B318** (1993) 237.

[13] CompHEP, *a System for Computations in High Energy Physics*, (1990-93), V. Savrin and S. Ilyin (Sc. Coord.), A. Pukhov (Comp.), E. Boos and M. Dubinin (Phys.), Moscow State Univ., Inst. for Nucl. Phys., Symb. Comp. Lab.; E. Boos et al., "New Computing Techniques in Phys. Research II", Proc. of

the 2^{nd} Int. Workshop on Software Engineering, Artificial Intelligence and Expert Systems in High Energy and Nuclear Physics, ed. D. Perret-Gallix World Scientific, 1992, p.665.

[14] G.P. Lepage, J. Comp. Phys. **27** (1978) 192.

[15] M. Jeżabek and J.H. Kühn, Nucl. Phys. **B314** (1989) 1; M. Jeżabek and J.H. Kühn, preprint TTP-93-4; A. Denner and T. Sack, Nucl. Phys. **B358** (1991) 46; G. Eilam, R.R. Mendel, R. Migneron and A. Soni, Phys. Rev. Lett. **66** (1991) 3105.

[16] J.H. Kühn, Acta Phys. Pol. **B12** (1981) 347; J.H. Kühn, Acta Phys. Austr. **Suppl.XXIV** (1982) 203; I. Bigi, Y.L. Dokshitzer, V.A. Khoze, J.H. Kühn and P.M. Zerwas, Phys. Lett. **B181** (1986) 157.

[17] V. Barger and R.J.N. Phillips, *"Collider Physics"*, ed. David Pines, 1987, p.268.

This figure "fig1-1.png" is available in "png" format from:

http://arXiv.org/ps/hep-ph/9311263v3

This figure "fig2-1.png" is available in "png" format from:

http://arXiv.org/ps/hep-ph/9311263v3

This figure "fig1-2.png" is available in "png" format from:

http://arXiv.org/ps/hep-ph/9311263v3

This figure "fig2-2.png" is available in "png" format from:

http://arXiv.org/ps/hep-ph/9311263v3

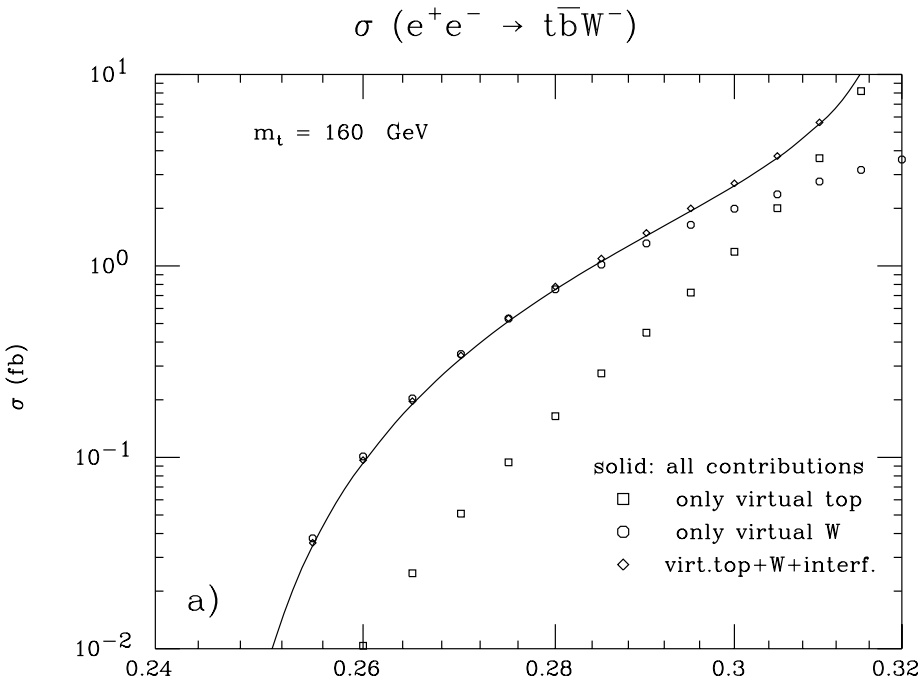
σ (e+e− → tb̄W−)
σ (fb)
10^1
10^0
10^−1
10^−2
0.24
0.26
0.28
0.3
0.32
m_t = 160 GeV
solid: all contributions
only virtual top
only virtual W
virt.top+W+interf.
a)

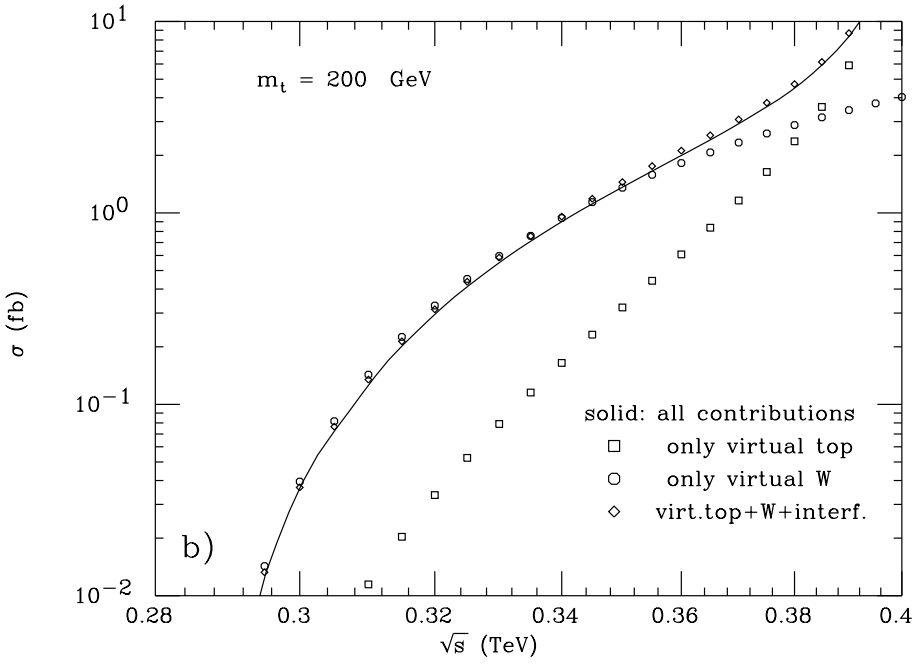
10^1
10^0
10^{-1}
10^{-2}
m_t = 200 GeV
b)
solid: all contributions
only virtual top
only virtual W
virt.top+W+interf.
σ (fb)
0.28
0.3
0.32
0.34
0.36
0.38
0.4
√s (TeV)

This figure "fig1-3.png" is available in "png" format from:

http://arXiv.org/ps/hep-ph/9311263v3

This figure "fig2-3.png" is available in "png" format from:

http://arXiv.org/ps/hep-ph/9311263v3

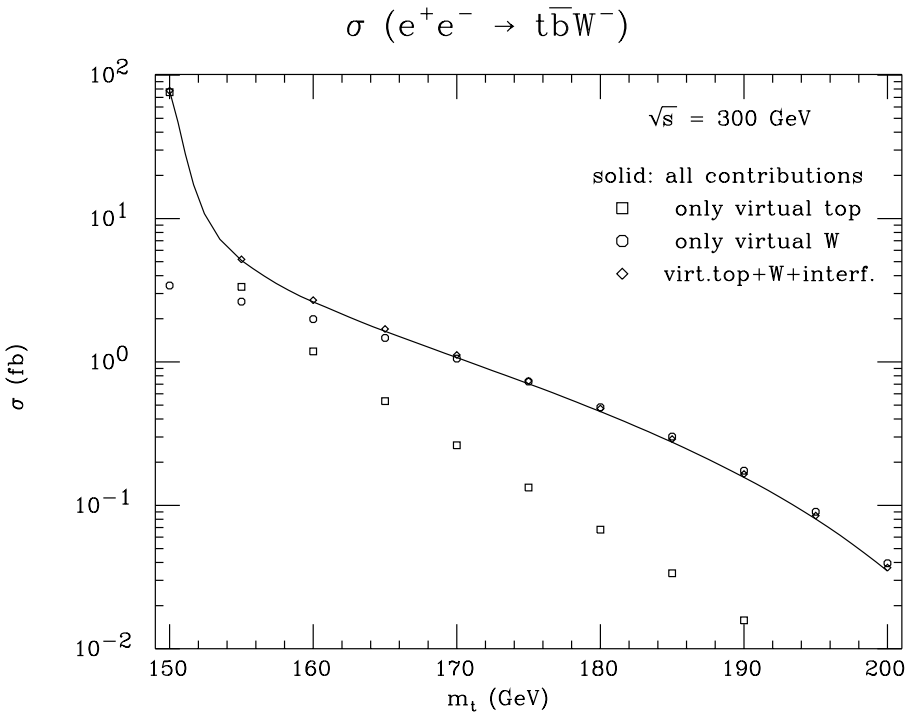
σ (e+e− → tb̄W−)
√s = 300 GeV
solid: all contributions
only virtual top
only virtual W
virt.top+W+interf.
σ (fb)
m_t (GeV)
10^2
10^1
10^0
10^−1
10^−2
150
160
170
180
190
200

This figure "fig1-4.png" is available in "png" format from:

http://arXiv.org/ps/hep-ph/9311263v3

This figure "fig2-4.png" is available in "png" format from:

http://arXiv.org/ps/hep-ph/9311263v3

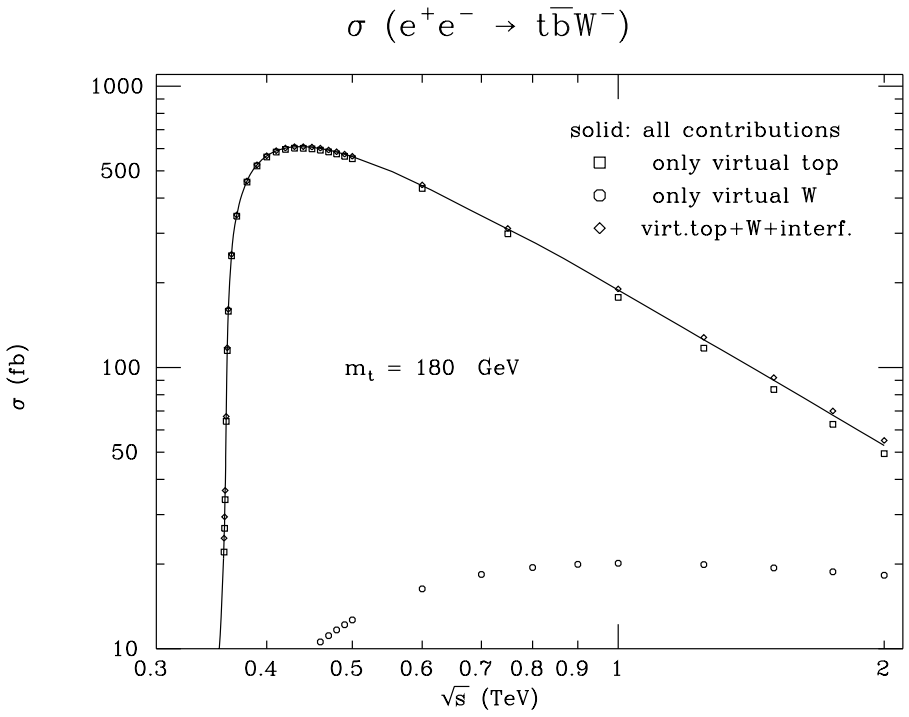
σ (e+e− → tb̄W−)
1000
500
100
50
10
σ (fb)
0.3
0.4
0.5
0.6
0.7
0.8
0.9
1
2
√s (TeV)
solid: all contributions
only virtual top
only virtual W
virt.top+W+interf.
mt = 180 GeV

This figure "fig1-5.png" is available in "png" format from:

http://arXiv.org/ps/hep-ph/9311263v3

This figure "fig2-5.png" is available in "png" format from:

http://arXiv.org/ps/hep-ph/9311263v3

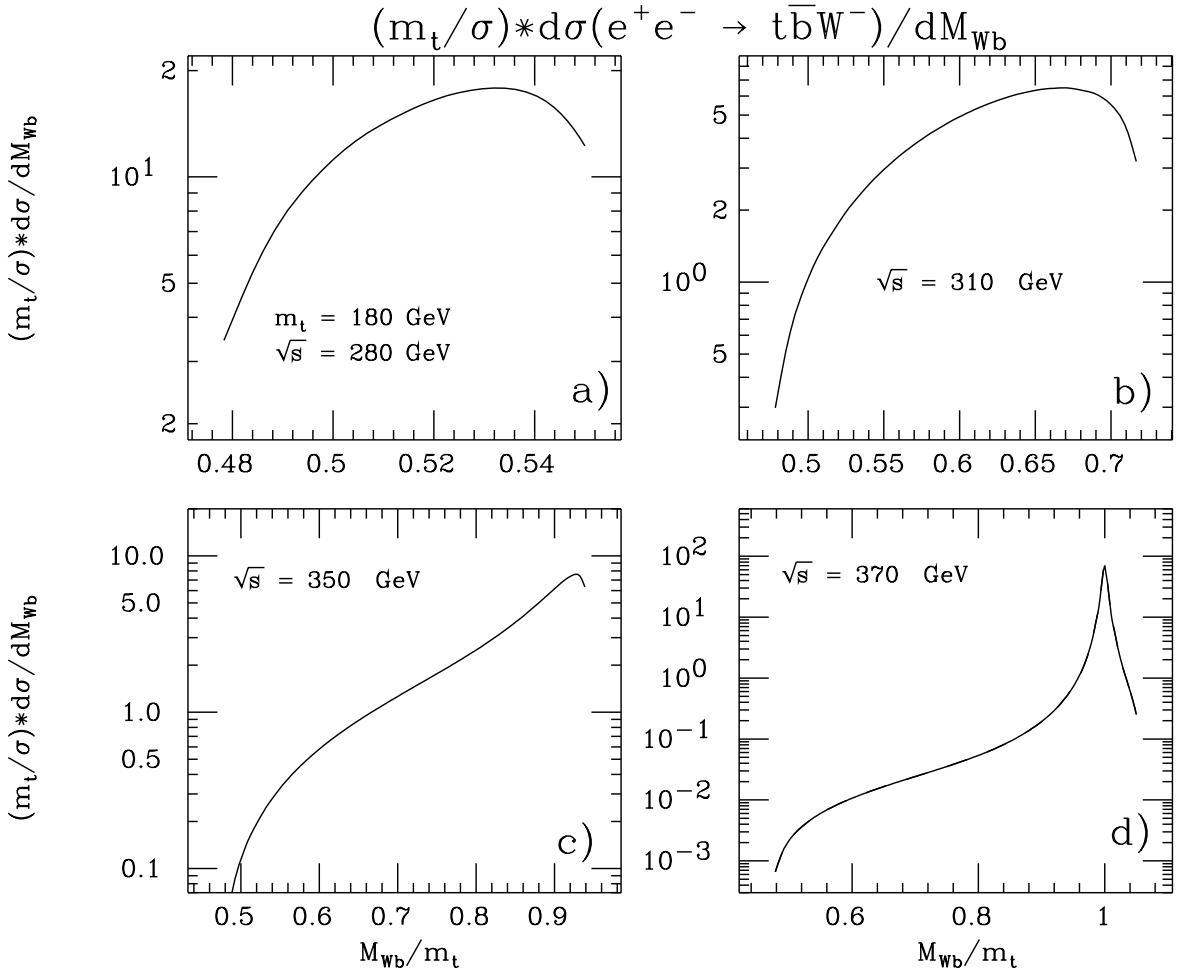
$(m_t/\sigma)*d\sigma(e^+e^- \to t\bar{b}W^-)/dM_{Wb}$
$(m_t/\sigma)*d\sigma/dM_{Wb}$
m_t = 180 GeV
$\sqrt{s}$ = 280 GeV
a)
$\sqrt{s}$ = 310 GeV
b)
$\sqrt{s}$ = 350 GeV
c)
$\sqrt{s}$ = 370 GeV
d)
M_{Wb}/m_t

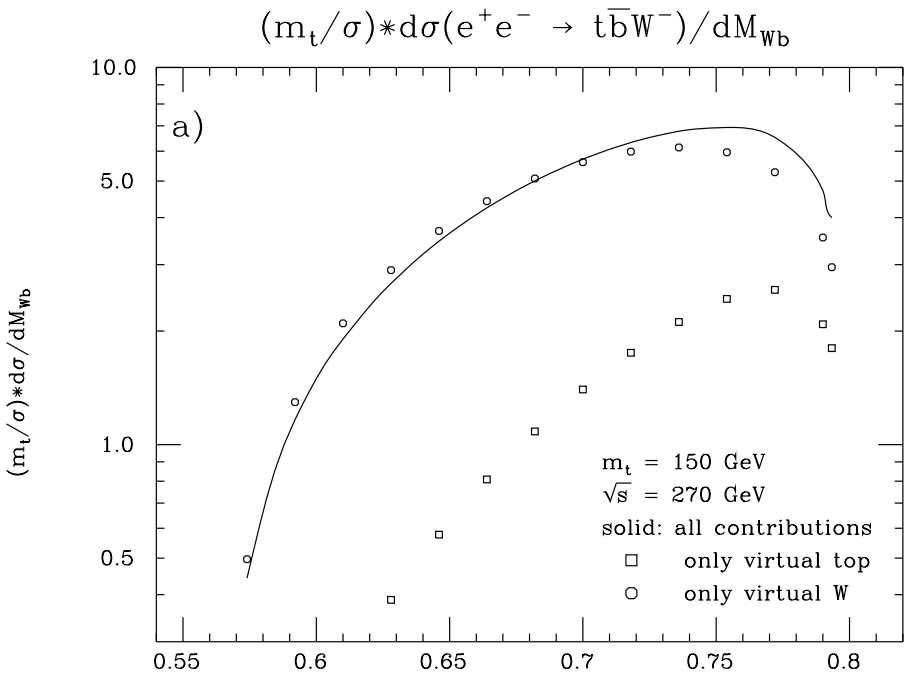
$(m_t/\sigma)*d\sigma(e^+e^- \to t\bar{b}W^-)/dM_{Wb}$
$(m_t/\sigma)*d\sigma/dM_{Wb}$
10.0
5.0
1.0
0.5
0.55
0.6
0.65
0.7
0.75
0.8
a)
m_t = 150 GeV
$\sqrt{s}$ = 270 GeV
solid: all contributions
only virtual top
only virtual W

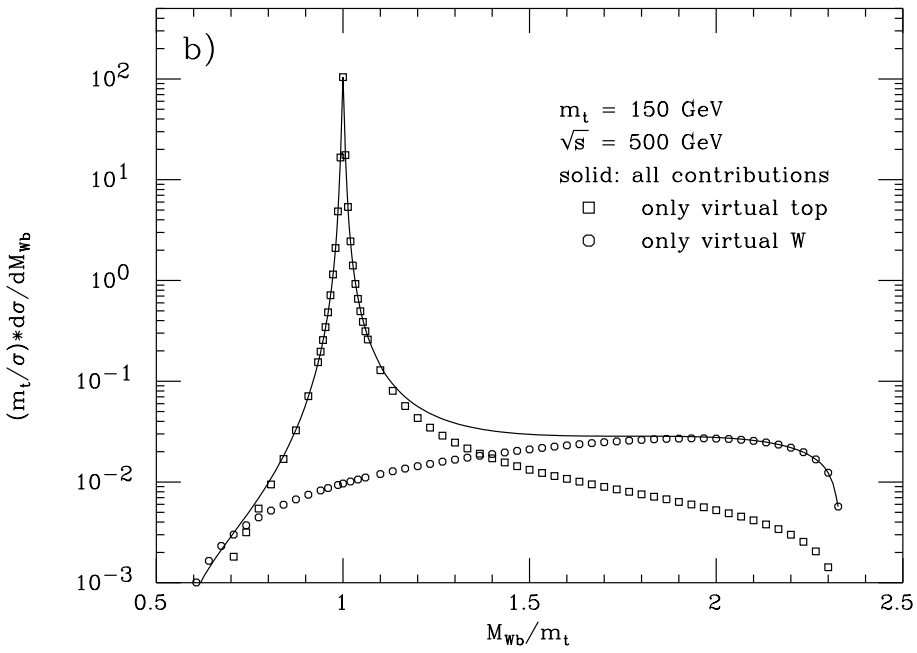
b)
m_t = 150 GeV
$\sqrt{s}$ = 500 GeV
solid: all contributions
only virtual top
only virtual W
$(m_t/\sigma)*d\sigma/dM_{Wb}$
M_{Wb}/m_t
10^2
10^1
10^0
10^{-1}
10^{-2}
10^{-3}
0.5
1
1.5
2
2.5

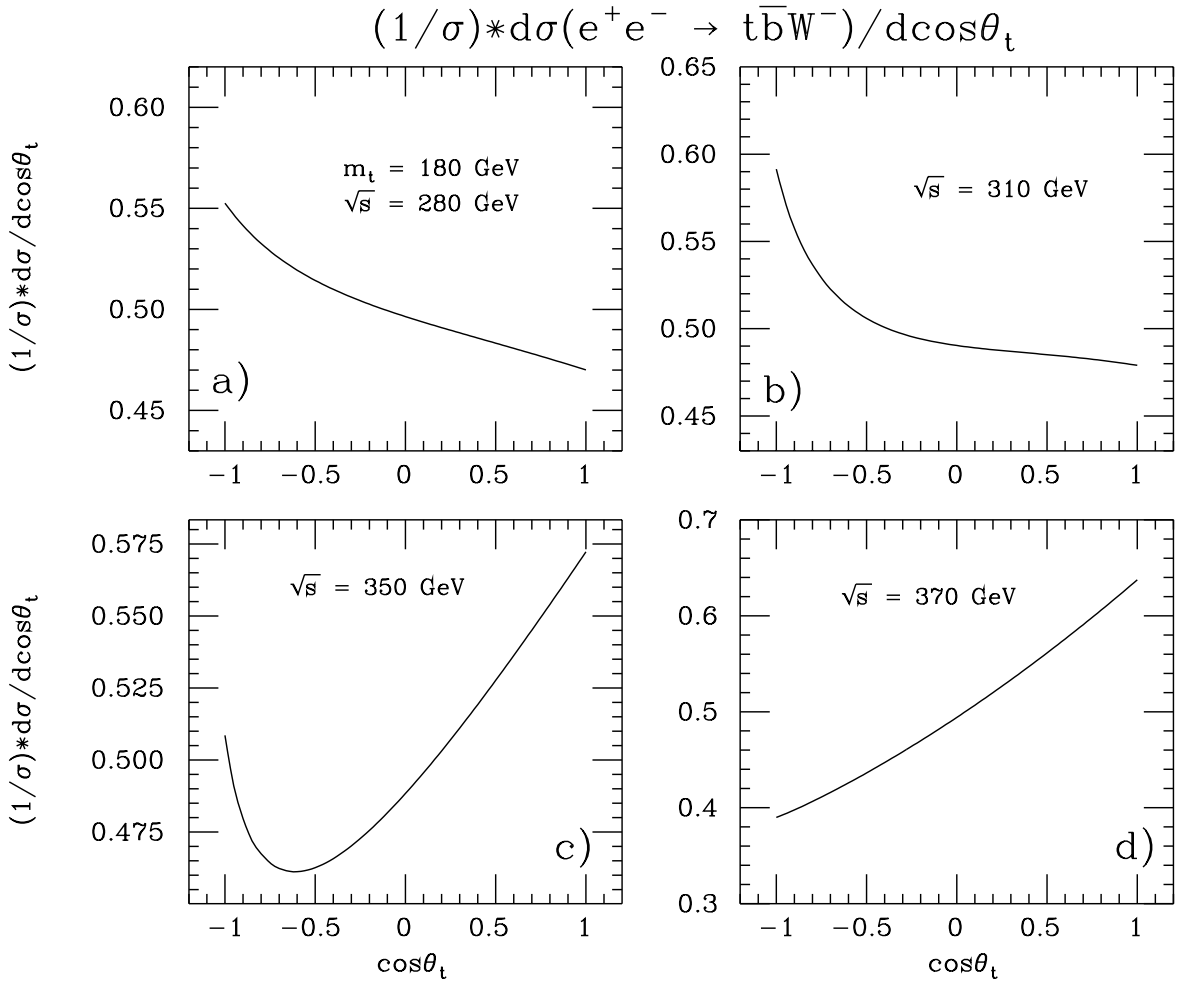
$(1/\sigma)*d\sigma(e^+e^- \to t\bar{b}W^-)/d\cos\theta_t$
$(1/\sigma)*d\sigma/d\cos\theta_t$
m_t = 180 GeV
$\sqrt{s}$ = 280 GeV
a)
$\sqrt{s}$ = 310 GeV
b)
$\sqrt{s}$ = 350 GeV
c)
$\sqrt{s}$ = 370 GeV
d)
$\cos\theta_t$

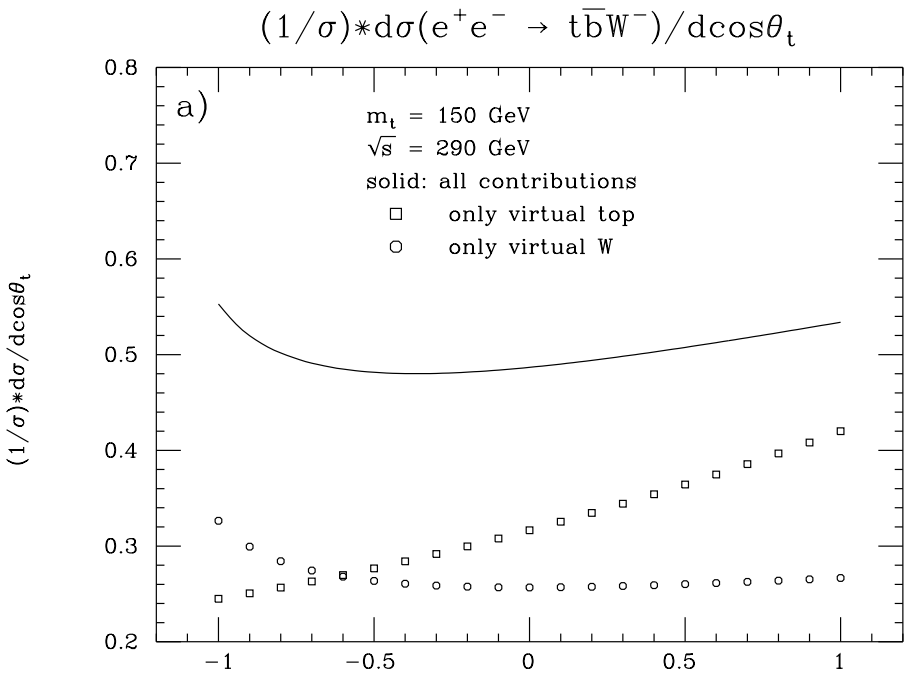
$(1/\sigma)*d\sigma(e^+e^- \to t\bar{b}W^-)/d\cos\theta_t$
a)
m_t = 150 GeV
$\sqrt{s}$ = 290 GeV
solid: all contributions
only virtual top
only virtual W
$(1/\sigma)*d\sigma/d\cos\theta_t$
0.8
0.7
0.6
0.5
0.4
0.3
0.2
−1
−0.5
0
0.5
1

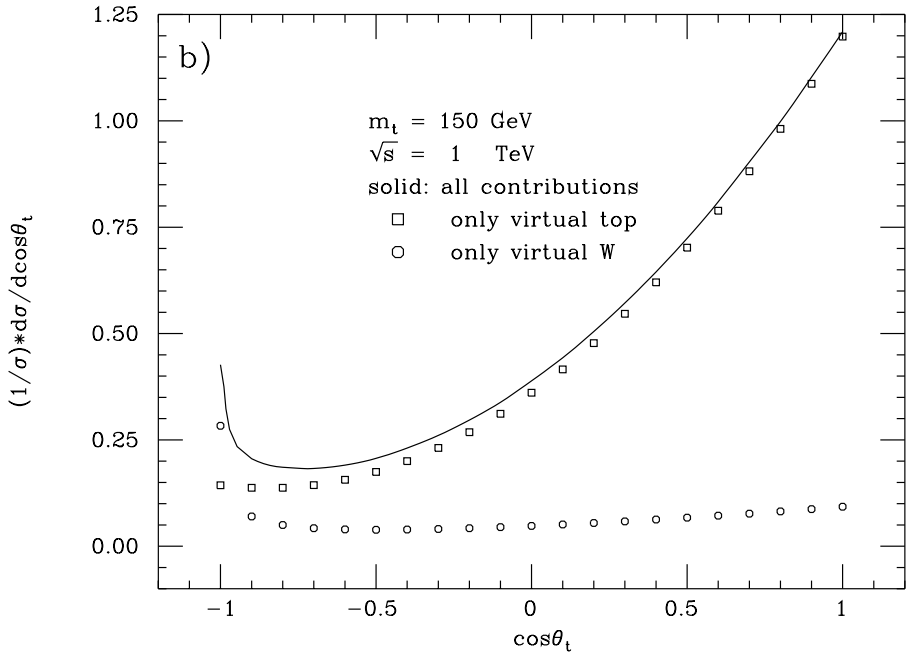
b)
m_t = 150 GeV
$\sqrt{s}$ = 1 TeV
solid: all contributions
only virtual top
only virtual W
$(1/\sigma)*d\sigma/d\cos\theta_t$
$\cos\theta_t$
1.25
1.00
0.75
0.50
0.25
0.00
−1
−0.5
0
0.5
1